Line-FRAP, a versatile method based on fluorescence recovery after photobleaching to measure diffusion rates *in vitro* and *in vivo*

Debabrata Dey, Shir Marciano and Gideon Schreiber

Department of Biomolecular Sciences, Weizmann Institute of Science

gideon.schreiber@weizmann.ac.il

Abstract

A cell is a densely packed conglomerate of macromolecules, where diffusion is essential for their function. The crowded conditions may affect diffusion both through hard (occluded space) and soft (weak, non-specific) interactions. Multiple-methods have been developed to measure diffusion rates at physiological protein concentrations within cells, however, each of them has its limitations. Here, we introduce Line-FRAP, a method based on measuring recovery of photobleaching under a confocal microscope that allows diffusion rate measurements in versatile environments using standard equipment. Implementation of Line mode to the classical FRAP technique improves the time resolution in data acquisition. We also introduce an updated method for data analysis. Together, these contribute towards better estimation of Diffusion coefficients in a wide range of environments. We evaluated the method using different proteins either chemically labelled or by fusion to YFP. The calculated diffusion rates were comparable to literature data as measured *in vitro*, using artificial crowders, in HeLa cells and in *E.coli*. Diffusion coefficients in HeLa was ~2.5-fold slower and in *E.coli* 15-fold slower than measured in buffer. Moreover, we show that increasing the osmotic pressure on *E.coli* further decreases diffusion by 2-3 fold. The method presented here is easy to apply on a standard confocal microscope, fits a large range of molecules with different sizes and provides robust results in any conceivable environment and protein concentration.

Introduction:

For cells to function, molecules of different sizes and composition diffuse in the crowded environment to reach their targets (Dix & Verkman, 2008; Goodsell, 1991; Verkman, 2002).

Fick's law, which predicts Diffusion driven by Brownian motion, is strictly valid for ideal solutions (with infinitely dilute concentrations of the solutes). It overlooks interactions between the moving species and with the surrounding (Agutter et al., 2000; Haugh, 2009; Saxton, 2012). Simulations and experiments describing molecular motions in a complex environment is a stiff challenge due to the various soft and hard interactions among the moving species (Baumann et al., 2010; Lenzi et al., 2016; Schavemaker et al., 2018). The classical theory of Stokes-Einstein regarding particle diffusion in ideal solution states that the diffusion constant of a particle *A* (D_A) is a function of its dimensions and the solution viscosity (Chandrasekhar, 1943; Einstein, 1905; Sutherland, 1905).

$$D_A = k_B T / 6\pi\eta r_A \qquad (1)$$

where η is the solvent viscosity, $k_B T$ is the product of the Boltzmann constant and the absolute temperature, r_A is the hydrodynamic radius of the diffusing particle and D_A is a measure of the mean squared displacements per unit time. (Sutherland, 1905) Interactions with other molecules that lower the mobility will be reflected by lower D_A values. Alternatively, if the motion of the molecule is increased because of the assistance from another faster moving dynamic molecule/surrounding environments, higher D_A values will be recorded. Both of these are known as anomalous diffusion (Haugh, 2009; Saxton, 2012). Accurate measurements of D_A values in the complex environment should correlate with the effective hydrodynamic radius, which takes into account the interactions the molecule is engaged in (Day & Kenworthy, 2009; He & Niemeyer, 2003; Mueller et al., 2010).

Over the years a wide range of different techniques have been developed to measure diffusion of different species inside the living cell. Most of these are fluorescent based. Among them, Fluorescence recovery after Photobleaching (FRAP) (Kitamura et al., 2015; Lippincott-Schwartz et al., 2003; Phair & Misteli, 2000; Verkman, 2003), fluorescence correlation microscopy (FCS) (Bacia et al., 2006; Cluzel et al., 2000; Dauty & Verkman, 2004; Ramadurai et al., 2009) and single particle tracking (SPT) (Manley et al., 2008) are the most popular. These techniques, separately or in combination, give reasonable diffusion values within the accepted ranges reported in the literature (Mika & Poolman, 2011; Miyawaki, 2011). Still, diffusion values reported by different research groups vary, predominantly inside the complex

environment of the cell (Kingsley et al., 2018). In addition, the assumptions of different mathematical models and imposed boundary conditions on the data processing of the different techniques can influence the results, which ultimately leads to a diversified range of diffusion values (Kingsley et al., 2018). Even for a specific molecule of interest using a single instrumental technique, diversified diffusion values create confusion and misunderstanding about the model and its underlying assumptions (Kingsley et al., 2018).

FCS is considered the gold standard for calculating diffusion coefficients in solution phase. However, it requires the measured particles to be very dilute (as low as ~1 - 10 nM), and a high quantum yield of the measured particle. This imposes sever limitations for measurements in crowded environments like inside the living cell. Moreover, if molecules have some bound fraction that is immobile, FCS remains completely blind to this fraction (Ries & Schwille, 2008; Wachsmuth, 2014). In addition, FCS has limitations regarding accurate detection of slowly binding molecules (Wachsmuth, 2014).

FRAP, is the most widely used technique by experimental biologists because of the relative ease of performing confocal FRAP in the majority of the biological domains. This technique is also very sensitive towards the bound or immobile fractions of the molecules under study (Costantini & Snapp, 2013; González-González et al., 2012; Hardy, 2012; Zuleger et al., 2013). However, there are major limitation associated with the FRAP technique. For one is the relative slow data accumulation rate, making it insensitive to fast diffusing particles (Wachsmuth, 2014). Second, the conversion of FRAP rates to D_A is problematic, and requires making multiple assumptions (Angelides et al., 1988; Axelrod et al., 1976; Braga et al., 2004; Deschout et al., 2010; Kang et al., 2009; Seiffert & Oppermann, 2005; Smisdom et al., 2011; Soumpasis, 1983; Sprague et al., 2004; Waharte et al., 2010). Here, we present a modified FRAP method to calculate D_A from *in vitro* to *in vivo* and provide robust diffusion data, similar to those determined using FCS. To overcome the slow data acquisition of the confocal microscope we devised a line-FRAP method, where a single scan along a line is repeated at ~1000 Hz. The use of two simultaneous scanners reduced the dead time of the instrument, resulting in further increase in efficiency of the line FRAP (Braeckmans et al., 2007). Careful evaluation of the size of the bleached area resulted in robust diffusion results for proteins and small molecules in varied conditions, including simple buffers, eukaryotic cells and the dense milieu of the bacterial cytoplasm under varying osmotic stresses.

Results

Theoretical background on extracting diffusing rates from FRAP data

Extracting diffusion coefficient values from FRAP recovery profiles is not straightforward (Angelides et al., 1988; Axelrod et al., 1976; Braga et al., 2004; Deschout et al., 2010; Kang et al., 2009; Seiffert & Oppermann, 2005; Smisdom et al., 2011; Soumpasis, 1983; Sprague et al., 2004; Waharte et al., 2010). The easiest way is to calculate half time of recovery ($\tau_{1/2}$) of the FRAP spot, which is defined as the time required for 50% recovery of the bleach spot (Lajoie et al., 2007; Salmon et al., 1984; Stricker et al., 2002; Zotter et al., 2017). Nevertheless, as also shown previously, $\tau_{1/2}$ measurements may actually be misleading, particularly as they do not take into account the processes occurring during bleach (Axelrod et al., 1976; Soumpasis, 1983). The classic equation derived by Soumpasis (Soumpasis, 1983) relating FRAP to the diffusion rate is:

$$Dr_n = 0.224\frac{r_n^2}{\tau_{1/2}} \quad (2)$$

This equation assumes a uniform radius of the bleach area (r_n) (Axelrod et al., 1976; Soumpasis, 1983). This relation is strictly valid for a pure isotropic diffusion model (Axelrod et al., 1976; Soumpasis, 1983). However, the main assumption i.e., diffusion during photobleaching is neglected, making its use for real FRAP experimental conditions limited. For normal laser scanning confocal microscopes, the relatively longer scanning durations increases the probability of significant amount of diffusions even during the photobleaching time pulse. This phenomenon obviously will be more common for faster diffusing molecules. Therefore, *D* values calculated from equation 2 can lead to underestimation of actual *D* in many systems (Braga et al., 2004; Kang et al., 2009; Pucadyil & Chattopadhyay, 2006; Weiss, 2004). Kang et.al. (Kang et al., 2012) solved these limitations by incorporating a new parameter, the effective bleach radius r_e. The final usable form of the modified equation is:

$$D_{confocal} = \frac{r_e^2+r_n^2}{8\tau_{1/2}} \quad (3)$$

When bleaching is instantaneous (i.e. for very short time pulse laser, $r_e = r_n$) $D = 0.25\frac{r_n^2}{\tau_{1/2}}$, which is similar to equation 2 (Kang et al., 2012). For the common case, where $r_e \neq r_n$ we determined experimentally r_e, r_n and $\tau_{1/2}$ in different conditions for line-FRAP, averaging 30

121 measurements for each sample and then using the effective bleach radius r_e in equation 3 to
122 determine $D_{confocal}$.

123

124 **Line FRAP Methodology**

125 Fig. 1A shows a pictorial representation of the Line-FRAP method performed in a life HeLa
126 cell expressing CFP (Cyan Fluorescent protein), showing both the fluorescence and
127 transmission Channels. The small red circle denotes the bleaching area, which is done by a Clip
128 tornado (of 4-pixel size, 1 pixel length equals to 0.207 micro meter) as defined by the Olympus
129 confocal system. The white line is the scanning line, which is performed at a rate of 800 Hz, to
130 follow FRAP as a function of time. As we record only a line, the method is named as Line-
131 FRAP (Braeckmans et al., 2007). Figure 1B shows the Line-FRAP cross section profile as a
132 function of time. The vertical direction of the line denotes the time progress. The vertical red
133 lines in the left panel shows the Region of Interest (ROI), from which the fluorescence intensity
134 over time is plotted (Figure 1C). The horizontal rectangular area marked as 1 (red color) in Fig.
135 1B right panel denotes the time frame immediate after the photo-bleach pulse (the highly
136 intense green is the bleach pulse). The time interval between each line measurement is 1.25
137 millisecond. The darker region reflects the bleached area. A typical example of a FRAP
138 recovery profile (averaged over 30 individual shots) is shown in Figure 1C. The red line denotes
139 fitting the data to a double exponential progression curve.

140 Several mathematical functions were tested to fit the FRAP recovery data. The bi-
141 exponential function gave a better fit than a single exponent function, not only in complex
142 environments but also in simple PBS buffer solution. The two-rate constant parameter k_1 and
143 k_2 with their associated amplitudes (a_1 and a_2) were used to calculate $\tau_{1/2}$ using equation 4.

144 $$\frac{1}{\tau_{1/2}} = \frac{p1}{\tau(1)_{1/2}} + \frac{p2}{\tau(2)_{1/2}} \qquad (4)$$

145 Where p_1 and p_2 are the fraction amplitudes of k_1 and k_2 and $\tau(1)_{1/2}$ $\tau(2)_{1/2}$ are the respective
146 half-recovery times. The reasons we observe more than one exponent in the recovery curve is
147 the diffusive boundary between the bleached area and its surrounding (Fig. 2). This relates
148 both to dispersion of the laser light and to diffusion occurring during the bleach time.

149 **Determination of r_n and r_e of the Bleach area**

Equation 3 is very sensitive to r_n and r_e values, which are squared, while $\tau_{1/2}$ is not. Kang et.al (Kang et al., 2012) estimated r in a slow diffusing system that allows 50 – 100 ms time lapses between frames. This is not relevant for fast diffusing systems, where recovery from bleach will occur within the first few frames. To obtain r_n values that are disconnected from diffusion we prepared a fluorescent protein sample that forms an aggregate. The sample consisted of BSA labelled with CF514 dye in PBS buffer and 30 percent (v/v) glycerol. Figure 2A shows Line FRAP profiles with corresponding fluorescence recovery over time traces for this sample. No FRAP were observed after photo bleach pulses of 10 ms and 63 ms. Figure 2B shows the bleach radius after 10, 20 and 63 ms of bleach pulses. The red circle is the set bleach of the laser (4 pixels). As seen, the size of the bleached area increases with increasing bleach times, which relates to the diffraction of the laser light, with the laser power set to 100% intensity in all cases(Kitamura & Kinjo, 2018). To quantify the signal, we plotted the intensity versus the position along the horizontal scanning line (Figure 2 C-E). To improve the signal to noise, we averaged 30 individual measurements and fitted them to a Gaussian (equation 5):

$$f_x = A^0 + Ae^{-\frac{(x-b)^2}{2c^2}} \quad (5)$$

where A^0 is the offset, A the amplitude, b the midpoint and c the width, which is related to the width at half maximum (FWHM) by FWHM = $2(2\ln 2)^{1/2}c$. Figure 2 (C-E) shows the Gaussian fits for post-bleach fluorescence profiles for 10, 20 and 63 ms of bleach pulses respectively.

Nominal radius values are assumed to be fixed for a given microscope setting and laser. Not so for the effective radius r_e, which depends also on the diffusion during bleach. Therefore it is mandatory to measure the effective bleach radius for each sample separately. Figure 3A shows Line-FRAP progression curves of BSA labelled with CF514 in PBS buffer, using 10 and 63 ms bleach pulse times. Figure 3B shows the fluorescence intensity along the horizontal line (after the photo bleach in Line-FRAP mode) for a single measurement. Figure 3C is an average of 30 measurements and figure 3D shows a gaussian fit of these data. Ambiguity remains over the percent recovery to be used for calculating r_n and r_e values. Kang et.al used 90% fluorescence signal recovery for r_e as the diameter of the effective bleach circle (Kang et al., 2012). However, this is an arbitrary choice, and therefore we preferred to obtain this value from equation 3 by comparing FRAP diffusion rates to those obtained by FCS for the same molecule. For this purpose we chose BSA, which diffusion rate has been estimated to be 63 and 51 $\mu m^2 s^{-1}$ using light scattering (Gaigalas et al., 1992), and FCS (Krouglova et al., 2004) measurements at 25ºC. Using the fitted c parameter in equation 5, we found that r_n and r_e should

182 be taken at 60% of total fluorescence signal recovery, which is equal to 1.38*c. Accordingly,
183 r_n values for 10, 20 and 63 ms bleach pulses calculated from the Gaussian fits are 0.745, 0.98
184 and 1.27 µm. These values show perfect agreement with the number of dark pixels present in
185 the Figure 2B. Table 1 shows the parameters used to obtain diffusion rates for BSA after 10
186 and 63 ms bleach times. While the bleach recovery rates and r_e are very different for 10 and 63
187 ms bleach time (Kitamura & Kinjo, 2018), the calculated diffusion coefficient is within 10%
188 from each other, and fit previous measurements (Gaigalas et al., 1992), (Krouglova et al., 2004).
189 Another outcome from this calibration experiment is that the calculation procedure remained
190 exactly the same, independent on whether 10 or 63 ms bleach time were used, despite the very
191 large differences in all measured parameters.

192 **Measuring BSA diffusion in crowded environments**

193 A rigorous test for the Line FRAP method is to retrieve diffusion rates in crowded
194 environments. PEG8000 is a synthetic polymer, popular for its use as crowder in solution
195 phase. Labelled BSA was added to 0, 5, 10, 15 and 20% (w/v) of PEG8000 in PBS buffer
196 solutions. The measurements were done after 10 and 63 ms bleach pulses. Figures 4 shows
197 FRAP recovery and post-bleach intensities for 10 ms (Figure 4A and 4B) and 63 ms (4C and
198 4D) bleach pulse durations. For r_n we used 0.745, 1.27 µm values for 10 and 63 ms bleach
199 pulses respectively. Values of r_e were calculated from Figure 4B and 4D using equation 5 as
200 detailed above. Values of $\tau_{1/2}$ were calculated using equation 4. The calculated diffusion
201 coefficients were plotted versus the relative solution viscosity (Figure 4E). The different fitted
202 parameters are provided in Table S1. As expected, the measured diffusion coefficients for BSA
203 in crowded environments showed a gradual decrease with increasing relative viscosity of the
204 PEG8000 solution (Kuttner et al., 2005). The measured diffusion values were (within the error)
205 the same, independent on whether 10 or 63 ms bleach times were used, despite the very
206 different recovery profiles. The results here show that Line-FRAP is capable for measuring
207 diffusion rates in different solutions with high reproducibility.

208 **Diffusion Coefficient Measurements *in vivo***

209 Our ultimate goal is to measure Diffusion Coefficients of proteins in the crowded milieu of the
210 cell. *In vivo* measurements introduce major technical challenges, including the variability
211 between individual living cells. Therefore, single-cell measurements should be performed in
212 sufficient numbers to estimate the diversity in terms of environments as well as sample
213 variations. Here, we used two bacterial proteins from *E.coli* origin, E-fts (PDB ID **1EFU)** and

214 baeR (PDB ID **4B09)** for our experiments. According to swiss model (Bertoni et al., 2017;
215 Waterhouse et al., 2018), E-fts and baeR are homodimers (dimer MW = 60.36 kDa and 55.2
216 kDa respectively). E-fts and baeR were labelled using two methods. One was with the CF514
217 fluorescent dye and the second by fusing the proteins to YFP (monomer MW, 26.4 kDa). We
218 have used the YFP protein variant with the A206K mutation to inhibit further oligomerization
219 of the YFP(Von Stetten et al., 2012). FRAP rates were first determined in PBS (Figure 5), from
220 which their respective diffusion coefficients were calculated as detailed above for BSA. The
221 diffusion coefficients of E-fts and baeR labelled with CF514 were 37.2 and 46 $\mu m^2 s^{-1}$
222 respectively. For the YFP fused proteins (with an estimated MW of 123 and 118 kDa) the
223 diffusion coefficients were as expected slower, 22.9 and 31.4 $\mu m^2 s^{-1}$ respectively (Table S2).

224 Next, we used these proteins to determine their diffusion coefficients in both Eukaryotic
225 and prokaryotic cells, as models for *in vivo* measurements. It is known that Eukaryotic cell
226 cytoplasm are less dense than prokaryotic cell cytoplasm, which should be reflected in the
227 diffusion coefficient (Dix & Verkman, 2008; Mika & Poolman, 2011). The 4 different proteins
228 (E-fts and baeR labelled with CF514 or fused to YFP) were microinjected inside HeLa cells
229 cytoplasm. Line-FRAP experiments were performed inside intact living cells (Figure. 6).
230 FRAP rates and r_e values were determined, from which the diffusion coefficients were
231 calculated (Table S2). As expected from the increased crowding of the cytoplasm of HeLa
232 cells, slower diffusion coefficients were determined(Dix & Verkman, 2008). For CF514
233 labelled proteins diffusion coefficients of 19.5 and 19 $\mu m^2 s^{-1}$ were determined for E-fts and
234 baeR respectively (Table S2). Diffusion coefficients of 9.0 and 12.5 $\mu m^2 s^{-1}$ were determined
235 for these proteins fused to YFP (which results in approximately doubling the MW).

236 *E.coli* bacterial cells are too small for micro-injection of proteins inside the cell (Mika
237 & Poolman, 2011). Hence, baeR-YFP and E-fts-YFP proteins were expressed in the bacterial
238 cell cytoplasm. To avoid fluorescence signal saturations, we have calibrated protein expression
239 levels using the *E.coli tuner* cells (Hartinger et al., 2010), where protein expression is tightly
240 regulated. A typical example of *E.coli* cells expressing YFP fused E-fts protein is shown in
241 Figure 7A. In Figure 7B and C FRAP recovery profiles of E-fts fused with YFP and baeR fused
242 with YFP in *E.coli* cytoplasm are shown. Figures 7D and E show the post-bleach fluorescens
243 intensity profiles, from which r_e values were calculated (Table S2). For the E-fts fused to YFP
244 D = 1.6 $\mu m^2 s^{-1}$ and for baeR fused to YFP D =0.95 $\mu m^2 s^{-1}$ were calculated (Table S2). In
245 addition, we have measured the diffusion coefficient of the YFP protein by itself in the
246 cytoplasm of *E.coli tuner* cells, resulting in a value of D = 4.6 $\mu m^2 s^{-1}$. Previously, a value of

247 7.7±2.5 $\mu m^2 s^{-1}$ was determined for GFP in *E.coli* D5Hα cells using photobleaching and photo
248 activation using conventional FRAP (Elowitz et al., 1999). It was further reported that GFP
249 diffusion rates depend on the expression level, with a value of D~ 3.6±0.7 $\mu m^2 s^{-1}$ being reported
250 at higher protein expression. Furthermore, insertion of a histidine tag during construct
251 designing resulted in D~ 4.0±2.0 $\mu m^2 s^{-1}$ (Elowitz et al., 1999). The published values indicate
252 that the Line-FRAP method predicts correctly diffusion coefficients in prokaryotic cells.
253 Moreover, the data qualities generated using Line-FRAP is less noisy than those shown in
254 previous reported FRAP measurements in *E.coli* (Elowitz et al., 1999; Kumar et al., 2010).

255 Figure 8 provides a comparison of diffusion coefficient values for E-fts and baeR in
256 different environments as determined using Line-FRAP. Fusing YFP doubles their MW, and
257 subsequently the diffusion coefficients were reduced in PBS buffer solution. Both the proteins
258 with YFP fusions showed further reduced mobility in the complex environment of the HeLa
259 cell cytoplasm. It is known that mammalian cell cytoplasm is 2-3 times as dense as aqueous
260 buffer solution (Dix & Verkman, 2008; Mika & Poolman, 2011). Prokaryotic cell cytoplasm
261 are further packed, with diffusion rates being over 10-fold slower than in buffer (Mika &
262 Poolman, 2011). The fold-change in diffusion coefficients from PBS to HeLa to *E.coli* is also
263 in line with the expected reduction due to the increased viscosity (Dix & Verkman, 2008; Mika
264 & Poolman, 2011).

265 To further test the validity of our Line-FRAP method, we have carried out Diffusion
266 rate measurements in *E.coli* cells under osmotically challenging environments. It is well known
267 that at higher osmotic stress, the cell wall starts to stretch causing the cytoplasm to shrink
268 (Konopka et al., 2009; Mika et al., 2014). As a consequence of the increased crowding density
269 inside the bacterial cell cytoplasm, the mobility of proteins slows down, which is reflected in
270 lower diffusion coefficient values (Konopka et al., 2009; Mika et al., 2014; Sochacki et al.,
271 2011). Figure 9A and B show normalized FRAP recovery profiles and corresponding post-
272 bleach profiles for YFP in *E.coli* under different osmotic stress conditions. Figure 9C shows a
273 comparison of the diffusion coefficient values under different osmotic conditions. Increasing
274 osmolarity was done by replacing the 2TY medium to HEPES buffer plus varying
275 concentrations of NaCl. This resulted in decreasing $D_{confocal}$ values, from D = 4.6 $\mu m^2 s^{-1}$ in 2TY
276 medium (including 85mM NaCl) to 3.2, 2.4 and 1.9 $\mu m^2 s^{-1}$ in presence of 150, 300 and 500
277 mM NaCl respectively (Table S3). These results confirm the power of the here presented
278 method in challenging conditions.

Our data show that we have developed a universal method by which one can compare diffusion coefficients measurements in different environments including *in vivo* by using FRAP. This allows diffusion measurements to be done using a simple, commonly available setup and applying straight forward data analysis tools. Moreover, protein-concentrations used for these measurements are in the μM range, which is in line with *in vivo* protein concentrations. Thus, the here presented system has major advantages over methods such as FCS in usability and versatility.

Experimental

Materials and Methods:

Dulbecco's phosphate buffered saline (PBS 1X) was purchased from Biological Industries (catalog no. 02-023-1A). CF514 fluorescent labelling dye was purchased from Biotium. All other reagents used are described in details in a table format (Table 2, Key resources)

Mammalian Cell culture

HeLa cells were grown in 35-mm glass-bottomed dishes (MatTek Corporation) in DMEM (Invitrogen) supplemented with 1x pyruvate, penicillin/streptomycin (BioLabs), and 10% fetal bovine serum (Equitech-BIO. Inc.). The cells were subcultured when 80% confluence was reached using trypsin-EDTA for cell detachment. $2x10^5$ HeLa cells in 2.5 ml of DMEM were pipetted into glass bottomed dishes and incubated overnight. The cells were cultured in humid atmosphere at 37 °C and 5% CO_2. The cells were imaged 24–30 h after the seeding process. Prior to the microinjection, the medium was aspirated, and the fresh medium was supplemented with 25 mM HEPES, pH 7.4.

Cloning and protein expression in E.coli

Three different constructs were cloned for BaeR and Efts. BaeR or Efts fused in their N-terminus to YFP (with A206K mutation that prevents self-dimerization) with a linker were cloned to pET21a plasmid. The same construct was cloned to pET28-his-sumo plasmid for purification. In addition, BaeR or Efts were cloned to pET28-his-sumo plasmid without YFP fusion. Cloning was done by RF cloning and by using a synthesized gene of YFP A206K (Twist biosciences). The YFP A206K BaeR or Efts in pET21a was transformed to Tuner™(DE3) Competent Cells (Novagene) which allow adjustable levels of protein expression throughout

309 all cells in a culture. They were grown in 37°C until they reached OD_{600}= 0.6 and induced by
310 adding IPTG to a final concentration of 0.1 mM in 37°C for three hours- then stored at 4°C
311 until imaging and measuring diffusion. For higher osmotic stress conditions, the YFP expressed
312 *E.coli* bacteria cells were centrifuged, and resuspended in 10 mM HEPES buffer solution (pH
313 7.2) with different NaCl salt concentrations (150-500 mM). The incubation time in buffer
314 solutions after resuspension was varied between 30 mins to 3 hours, which had to effect on the
315 calculated diffusing rates. For protein-purification, YFP A206K BaeR or Efts in pET28-his-
316 sumo and BaeR or Efts in pET28-his-sumo plasmid were transformed to BL21 (DE3)
317 competent cells. They were grown at 37°C until they reached OD_{600}= 0.6-0.8 before adding 0.1
318 mM IPTG for protein production in 16°C overnight.

319 ***Protein Purification***

320 After overnight growth, the cells were harvested for 10 minutes at 5000 rpm and stored at -
321 20°C. The pellets were resuspended in 50 mM Tris-HCl, 200 mM NaCl and 10 mM Imidazole
322 pH=8 buffer. Protease inhibitor, lysozyme and benzonase were added. After homogenization,
323 sonication was done by using 3 cycles of 10 seconds on and 30 seconds off keeping the sample
324 on ice. Then, the samples were centrifuged at 14000 rpm for 60 minutes at 4°C. The supernatant
325 was used for further purification. Ni-NTA gravity columns of 200 ul Ni-NTA (Merck) were
326 equilibrated with binding buffer containing 50 mM Tris-HCl pH=8, 200 mM NaCl, 10 mM
327 Imidazole and 10% glycerol. The supernatant was loaded onto the column after 0.45 nm
328 filtration (Millex-HV; Millipore), then, washed with 50 mM Tris-HCl, 200 mM NaCl, 20 mM
329 Imidazole and 10% glycerol twice. On column cleavage was done by sumo-protease in elution
330 buffer: 50 mM Tris-HCl, 200 mM NaCl, 10% glycerol, 1mM DTT, 1:200 sumo protease. The
331 cleavage was done one hour in room temp and then overnight at 4°C under constant rotation.
332 Elution from beads was done twice using the cleavage buffer. For BaeR and Efts this was
333 followed by anion exchange of a FF Q column (GE). Purified proteins were analyzed by SDS-
334 PAGE gel-electrophoresis and its concentrations were determined using a nanodrop. The
335 purified protein was dialyzed using midi-gebaflex 3.5 kDa (Geba) against 0.1M $NaHCO_3$
336 buffer that is compatible to labelling with CF514 dye. The protein was then aliquoted, flash-
337 frozen in liquid nitrogen, and stored at -80°C.

338 ***Protein labelling with CF514***

339 The purified BaeR and Efts were labelled with CF514 dye (Biotium) according to the
340 manufacturer recommendations. Labelled proteins were dialyzed against PBS using Gebaflex

341 3.5KDa (GeBa) and further purified from the dye using Pierce™ Dye Removal Columns
342 (Cat#22858, Thermo-Fisher scientific).

343 ***Microinjection into HeLa cells***

344 Microinjections were performed using Eppendorf FemtoJet microinjector attached to
345 Eppendorf InjectMan NI2 micromanipulator. The different fluorescent proteins were dissolved
346 in PBS and injected into cells using glass capillaries from Warner instruments and pulled by
347 vertical puller (Narishige). For every measurement, a single pressure pulse was applied to
348 deliver the sample into the cell. Air was administrated at 15– 25 hPa for 0.1-0.3 s. For
349 injections, single cells containing morphologically healthy and well-connected HeLa cells were
350 selected. Before and after the microinjection, cell morphology and the membrane integrity were
351 confirmed by visually inspecting the injected cells.

352 ***Confocal microscopy and FRAP Analysis:***

353 *Confocal microscopy.* Imaged were collected with an Olympus IX81 FluoView FV1000
354 Spectral/SIM Scanner confocal laser-scanning microscope, using 60X DIC oil-immersion
355 objective, N.A. 1.35. For CF514/YFP fluorescence measurements, excitation was done at 515-
356 nm, using a diode laser at an output power of 3% and 1% for low and high YFP/CF514 dye
357 concentrations. Emission was recorded from 530 to 630 nm using the spectral detection system.
358 All image analyses were performed using FluoView software and data analyses were
359 performed using Kaleidagraph software version 4.1 (Synergy).

360 ***Line-FRAP***

361 Line-FRAP was carried out in liquid drops, HeLa cells or *E.coli*. The target cells were imaged
362 with the main scanner at 515-nm excitation using 3% of the maximal intensity applying a 60x
363 differential interference contrast oil-immersion objective lens. For photobleaching, a "tornado"
364 of 4 pixels diameter was used in the simultaneous stimulus scanner. The circle area of the
365 bleach was kept exactly in the middle of the scanning line. The unidirectional lines were
366 scanned with time intervals of 1.256 ms 1000 times (equivalent to 1.256 s). The number of
367 scans before, during, and after photobleaching was 10, 42, and 948, respectively.
368 Photobleaching was achieved with the simultaneous laser at 405-nm excitation for 10 or 63
369 milisecond duration, using full intensity. The simultaneous scanner moved at a speed of 100
370 µs/pixel to perform an efficient photobleach. We have used two simultaneous scanners during
371 the FRAP experiments: one scanner (at 405 nm) for photobleaching and another scanner (at

515 nm) for data acquisition. We have varied the intensity of the lasers to achieve good signal/noise ratio. Fluorescence recovery plots were fitted to a double exponent growth curve. To do a comparative study, FRAP experiments were also performed inside the PBS buffer drops putting a cover slip upside like in a sandwich mode.

ACKNOWLEDGMENT

We would like to thanks Dr. Hagen Hofmann from the department of structural biology, Weizmann Institute of Science for advice and critically reading the manuscript, and Dr. Vladimir Kiss from the department of biomolecular sciences for his help in the microscopy work. The work was supported by a grant of the Israel Science Foundation number 1268/18 and a grant by the United States - Israel Binational Science Foundation number 2015376.

REFERENCES:

1. Goodsell, D. S. (1991). Inside a living cell. *Trends in Biochemical Sciences*, *16*(C), 203–206. https://doi.org/10.1016/0968-0004(91)90083-8
2. Verkman, A. S. (2002). Solute and macromolecule diffusion in cellular aqueous compartments. In *Trends in Biochemical Sciences* (Vol. 27, Issue 1, pp. 27–33). https://doi.org/10.1016/S0968-0004(01)02003-5
3. Dix, J. A., & Verkman, A. S. (2008). Crowding Effects on Diffusion in Solutions and Cells. *Annual Review of Biophysics*, *37*(1), 247–263. https://doi.org/10.1146/annurev.biophys.37.032807.125824
4. Agutter, P. S., Malone, P. C., & Wheatley, D. N. (2000). Diffusion theory in biology: A relic of mechanistic materialism. *Journal of the History of Biology*, *33*(1), 71–111. https://doi.org/10.1023/A:1004745516972
5. Haugh, J. M. (2009). Analysis of reaction-diffusion systems with anomalous subdiffusion. *Biophysical Journal*, *97*(2), 435–442. https://doi.org/10.1016/j.bpj.2009.05.014
6. Saxton, M. J. (2012). Wanted: A positive control for anomalous subdiffusion. In *Biophysical Journal* (Vol. 103, Issue 12, pp. 2411–2422). https://doi.org/10.1016/j.bpj.2012.10.038
7. Baumann, G., F. Place, R., & Foldes-Papp, Z. (2010). Meaningful Interpretation of Subdiffusive Measurements in Living Cells (Crowded Environment) by Fluorescence Fluctuation Microscopy. *Current Pharmaceutical Biotechnology*, *11*(5), 527–543. https://doi.org/10.2174/138920110791591454
8. Lenzi, E. K., Ribeiro, H. V., Tateishi, A. A., Zola, R. S., & Evangelista, L. R. (2016). Anomalous diffusion and transport in heterogeneous systems separated by a membrane. *Proceedings of the Royal Society A: Mathematical, Physical and Engineering Sciences*, *472*(2195). https://doi.org/10.1098/rspa.2016.0502

9. Schavemaker, P. E., Boersma, A. J., & Poolman, B. (2018). How important is protein diffusion in prokaryotes? In *Frontiers in Molecular Biosciences* (Vol. 5, Issue NOV). https://doi.org/10.3389/fmolb.2018.00093
10. Einstein, A. (1905). on the Movement of Small Particles Suspended in a Stationary Liquid Demanded By the Molecular- Kinetic Theory of Heat. *Annalen Der Physik*, *322*(8), 549–560. https://doi.org/10.1002/andp.19053220806
11. Sutherland, W. (1905). LXXV. A dynamical theory of diffusion for non-electrolytes and the molecular mass of albumin . *The London, Edinburgh, and Dublin Philosophical Magazine and Journal of Science*, *9*(54), 781–785. https://doi.org/10.1080/14786440509463331
12. Chandrasekhar, S. (1943). Stochastic problems in physics and astronomy. *Reviews of Modern Physics*, *15*(1), 1–89. https://doi.org/10.1103/RevModPhys.15.1
13. Mueller, F., Mazza, D., Stasevich, T. J., & McNally, J. G. (2010). FRAP and kinetic modeling in the analysis of nuclear protein dynamics: What do we really know? In *Current Opinion in Cell Biology* (Vol. 22, Issue 3, pp. 403–411). https://doi.org/10.1016/j.ceb.2010.03.002
14. Day, C. A., & Kenworthy, A. K. (2009). Tracking microdomain dynamics in cell membranes. In *Biochimica et Biophysica Acta - Biomembranes* (Vol. 1788, Issue 1, pp. 245–253). https://doi.org/10.1016/j.bbamem.2008.10.024
15. He, L., & Niemeyer, B. (2003). A novel correlation for protein diffusion coefficients based on molecular weight and radius of gyration. *Biotechnology Progress*, *19*(2), 544–548. https://doi.org/10.1021/bp0256059
16. He, L., & Niemeyer, B. (2003). A novel correlation for protein diffusion coefficients based on molecular weight and radius of gyration. *Biotechnology Progress*, *19*(2), 544–548. https://doi.org/10.1021/bp0256059
17. Verkman, A. S. (2003). Diffusion in cells measured by fluorescence recovery after photobleaching. *Methods in Enzymology*, *360*, 635–648. https://doi.org/10.1016/S0076-6879(03)60132-1
18. Lippincott-Schwartz, J., Altan-Bonnet, N., & Patterson, G. H. (2003). Photobleaching and photoactivation: Following protein dynamics in living cells. In *Nature Reviews Molecular Cell Biology* (Vol. 4, Issue SUPPL.).
19. Kitamura, A., Nakayama, Y., & Kinjo, M. (2015). Efficient and dynamic nuclear localization of green fluorescent protein via RNA binding. *Biochemical and Biophysical Research Communications*, *463*(3), 401–406. https://doi.org/10.1016/j.bbrc.2015.05.084
20. Bacia, K., Kim, S. A., & Schwille, P. (2006). Fluorescence cross-correlation spectroscopy in living cells. *Nature Methods*, *3*(2), 83–89. https://doi.org/10.1038/nmeth822
21. Dauty, E., & Verkman, A. S. (2004). Molecular crowding reduces to a similar extent the diffusion of small solutes and macromolecules: Measurement by fluorescence correlation spectroscopy. *Journal of Molecular Recognition*, *17*(5), 441–447. https://doi.org/10.1002/jmr.709
22. Ramadurai, S., Holt, A., Krasnikov, V., Van Den Bogaart, G., Killian, J. A., & Poolman, B. (2009). Lateral diffusion of membrane proteins. *Journal of the American Chemical Society*, *131*(35), 12650–12656. https://doi.org/10.1021/ja902853g
23. Cluzel, P., Surette, M., & Leibler, S. (2000). An ultrasensitive bacterial motor revealed by monitoring signaling proteins in single cells. *Science*, *287*(5458), 1652–1655. https://doi.org/10.1126/science.287.5458.1652
24. Manley, S., Gillette, J. M., Patterson, G. H., Shroff, H., Hess, H. F., Betzig, E., & Lippincott-Schwartz, J. (2008). High-density mapping of single-molecule trajectories

with photoactivated localization microscopy. *Nature Methods*, *5*(2), 155–157. https://doi.org/10.1038/nmeth.1176

25. Mika, J. T., & Poolman, B. (2011). Macromolecule diffusion and confinement in prokaryotic cells. In *Current Opinion in Biotechnology* (Vol. 22, Issue 1, pp. 117–126). https://doi.org/10.1016/j.copbio.2010.09.009
26. Miyawaki, A. (2011). Proteins on the move: Insights gained from fluorescent protein technologies. In *Nature Reviews Molecular Cell Biology* (Vol. 12, Issue 10, pp. 656–668). https://doi.org/10.1038/nrm3199
27. Kingsley, J. L., Bibeau, J. P., Mousavi, S. I., Unsal, C., Chen, Z., Huang, X., Vidali, L., & Tuzel, E. (2018). Understanding Boundary Effects and Confocal Optics Enables Quantitative FRAP Analysis in the Confined Geometries of Animal, Plant and Fungal Cells. *Biophysical Journal*, *114*(3), 349a-350a. https://doi.org/10.1016/j.bpj.2017.11.1948
28. Ries, J., & Schwille, P. (2008). New concepts for fluorescence correlation spectroscopy on membranes. In *Physical Chemistry Chemical Physics* (Vol. 10, Issue 24, pp. 3487–3497). https://doi.org/10.1039/b718132a
29. Wachsmuth, M. (2014). Molecular diffusion and binding analyzed with FRAP. In *Protoplasma* (Vol. 251, Issue 2, pp. 373–382). https://doi.org/10.1007/s00709-013-0604-x
30. González-González, I. M., Jaskolski, F., Goldberg, Y., Ashby, M. C., & Henley, J. M. (2012). Measuring membrane protein dynamics in neurons using fluorescence recovery after photobleach. In *Methods in Enzymology* (Vol. 504, pp. 127–146). https://doi.org/10.1016/B978-0-12-391857-4.00006-9
31. Hardy, L. R. (2012). Fluorescence recovery after photobleaching (FRAP) with a focus on F-actin. *Current Protocols in Neuroscience*, *SUPPL.61*. https://doi.org/10.1002/0471142301.ns0217s61
32. Costantini, L., & Snapp, E. (2013). Probing endoplasmic reticulum dynamics using fluorescence imaging and photobleaching techniques. *Current Protocols in Cell Biology*, *SUPPL.60*. https://doi.org/10.1002/0471143030.cb2107s60
33. Zuleger, N., Kelly, D. A., & Schirmer, E. C. (2013). Considering discrete protein pools when measuring the dynamics of nuclear membrane proteins. *Methods in Molecular Biology*, *1042*, 275–298. https://doi.org/10.1007/978-1-62703-526_2
34. Axelrod, D., Koppel, D. E., Schlessinger, J., Elson, E., & Webb, W. W. (1976). Mobility measurement by analysis of fluorescence photobleaching recovery kinetics. *Biophysical Journal*, *16*(9), 1055–1069. https://doi.org/10.1016/S0006-3495(76)85755-4
35. Soumpasis, D. M. (1983). Theoretical analysis of fluorescence photobleaching recovery experiments. *Biophysical Journal*, *41*(1), 95–97. https://doi.org/10.1016/S0006-3495(83)84410-5
36. Kang, M., Day, C. A., Drake, K., Kenworthy, A. K., & DiBenedetto, E. (2009). A generalization of theory for two-dimensional fluorescence recovery after photobleaching applicable to confocal laser scanning microscopes. *Biophysical Journal*, *97*(5), 1501–1511. https://doi.org/10.1016/j.bpj.2009.06.017
37. Braga, J., Desterro, J. M. P., & Carmo-Fonseca, M. (2004). Intracellular macromolecular mobility measured by fluorescence recovery after photobleaching with confocal laser scanning microscopes. *Molecular Biology of the Cell*, *15*(10), 4749–4760. https://doi.org/10.1091/mbc.E04-06-0496
38. Angelides, K. J., Elmer, L. W., Loftus, D., & Elson, E. (1988). Distribution and lateral mobility of voltage-dependent sodium channels in neurons. *Journal of Cell Biology*, *106*(6), 1911–1925. https://doi.org/10.1083/jcb.106.6.1911

39. Seiffert, S., & Oppermann, W. (2005). Systematic evaluation of FRAP experiments performed in a confocal laser scanning microscope. *Journal of Microscopy*, *220*(1), 20–30. https://doi.org/10.1111/j.1365-2818.2005.01512.x
40. Sprague, B. L., Pego, R. L., Stavreva, D. A., & McNally, J. G. (2004). Analysis of binding reactions by fluorescence recovery after photobleaching. *Biophysical Journal*, *86*(6), 3473–3495. https://doi.org/10.1529/biophysj.103.026765
41. Deschout, H., Hagman, J., Fransson, S., Jonasson, J., Rudemo, M., Lorén, N., & Braeckmans, K. (2010). Straightforward FRAP for quantitative diffusion measurements with a laser scanning microscope. *Optics Express*, *18*(22), 22886. https://doi.org/10.1364/oe.18.022886
42. Waharte, F., Steenkeste, K., Briandet, R., & Fontaine-Aupart, M. P. (2010). Diffusion measurements inside biofilms by image-based fluorescence recovery after photobleaching (FRAP) analysis with a commercial confocal laser scanning microscope. *Applied and Environmental Microbiology*, *76*(17), 5860–5869. https://doi.org/10.1128/AEM.00754-10
43. Smisdom, N., Braeckmans, K., Deschout, H., vandeVen, M., Rigo, J.-M., De Smedt, S. C., & Ameloot, M. (2011). Fluorescence recovery after photobleaching on the confocal laser-scanning microscope: generalized model without restriction on the size of the photobleached disk. *Journal of Biomedical Optics*, *16*(4), 046021. https://doi.org/10.1117/1.3569620
44. Braeckmans, K., Remaut, K., Vandenbroucke, R. E., Lucas, B., De Smedt, S. C., & Demeester, J. (2007). Line FRAP with the confocal laser scanning microscope for diffusion measurements in small regions of 3-D samples. *Biophysical Journal*, *92*(6), 2172–2183. https://doi.org/10.1529/biophysj.106.099838
45. Stricker, J., Maddox, P., Salmon, E. D., & Erickson, H. P. (2002). Rapid assembly dynamics of the Escherichia coli FtsZ-ring demonstrated by fluorescence recovery after photobleaching. *Proceedings of the National Academy of Sciences of the United States of America*, *99*(5), 3171–3175. https://doi.org/10.1073/pnas.052595099
46. Salmon, E. D., Leslie, R. J., Saxton, W. M., Karow, M. L., & McIntosh, J. R. (1984). Spindle microtubule dynamics in sea urchin embryos: Analysis using a fluorescein-labeled tubulin and measurements of fluorescence redistribution after laser photobleaching. *Journal of Cell Biology*, *99*(6), 2165–2174. https://doi.org/10.1083/jcb.99.6.2165
47. Lajoie, P., Partridge, E. A., Guay, G., Goetz, J. G., Pawling, J., Lagana, A., Bharat, J., Dennis, J. W., & Nabi, I. R. (2007). Plasma membrane domain organization regulates EGFR signaling in tumor cells. *Journal of Cell Biology*, *179*(2), 341–356. https://doi.org/10.1083/jcb.200611106
48. Zotter, A., Bäuerle, F., Dey, D., Kiss, V., & Schreiber, G. (2017). Quantifying enzyme activity in living cells. *Journal of Biological Chemistry*, *292*(38), 15838–15848. https://doi.org/10.1074/jbc.M117.792119
49. Weiss, M. (2004). Challenges and artifacts in quantitative photobleaching experiments. *Traffic*, *5*(9), 662–671. https://doi.org/10.1111/j.1600-0854.2004.00215.x
50. Pucadyil, T. J., & Chattopadhyay, A. (2006). Confocal fluorescence recovery after photobleaching of green fluorescent protein in solution. *Journal of Fluorescence*, *16*(1), 87–94. https://doi.org/10.1007/s10895-005-0019-y
51. Kang, M., Day, C. A., Kenworthy, A. K., & DiBenedetto, E. (2012). Simplified equation to extract diffusion coefficients from confocal FRAP data. *Traffic*, *13*(12), 1589–1600. https://doi.org/10.1111/tra.12008

52. Kitamura, A., & Kinjo, M. (2018). Determination of diffusion coefficients in live cells using fluorescence recovery after photobleaching with wide-field fluorescence microscopy.*Biophysics and Physicobiology*, *15*(0), 1–7. https://doi.org/10.2142/biophysico.15.0_1
53. Gaigalas, A. K., Hubbard, J. B., McCurley, M., & Woo, S. (1992). Diffusion of bovine serum albumin in aqueous solutions. *Journal of Physical Chemistry*, *96*(5), 2355–2359. https://doi.org/10.1021/j100184a063
54. Krouglova, T., Vercammen, J., & Engelborghs, Y. (2004). Correct diffusion coefficients of proteins in fluorescence correlation spectroscopy. Application to tubulin oligomers induced by Mg2+ and Paclitaxel. *Biophysical Journal*, *87*(4), 2635–2646. https://doi.org/10.1529/biophysj.104.040717
55. Kuttner, Y. Y., Kozer, N., Segal, E., Schreiber, G., & Haran, G. (2005). Separating the contribution of translational and rotational diffusion to protein association. *Journal of the American Chemical Society*, *127*(43), 15138–15144. https://doi.org/10.1021/ja053681c
56. Bertoni, M., Kiefer, F., Biasini, M., Bordoli, L., & Schwede, T. (2017). Modeling protein quaternary structure of homo- and hetero-oligomers beyond binary interactions by homology. *Scientific Reports*, *7*(1). https://doi.org/10.1038/s41598-017-09654-8
57. Waterhouse, A., Bertoni, M., Bienert, S., Studer, G., Tauriello, G., Gumienny, R., Heer, F. T., De Beer, T. A. P., Rempfer, C., Bordoli, L., Lepore, R., & Schwede, T. (2018). SWISS-MODEL: Homology modelling of protein structures and complexes. *Nucleic Acids Research*, *46*(W1), W296–W303. https://doi.org/10.1093/nar/gky427
58. Von Stetten, D., Noirclerc-Savoye, M., Goedhart, J., Gadella, T. W. J., & Royant, A. (2012). Structure of a fluorescent protein from Aequorea victoria bearing the obligate-monomer mutation A206K. *Acta Crystallographica Section F: Structural Biology and Crystallization Communications*, *68*(8), 878–882. https://doi.org/10.1107/S1744309112028667
59. Hartinger, D., Heinl, S., Schwartz, H. E., Grabherr, R., Schatzmayr, G., Haltrich, D., & Moll, W. D. (2010). Enhancement of solubility in Escherichia coli and purification of an aminotransferase from Sphingopyxis sp. MTA144 for deamination of hydrolyzed fumonisin B1. *Microbial Cell Factories*, *9*. https://doi.org/10.1186/1475-2859-9-62
60. Hartinger, D., Heinl, S., Schwartz, H. E., Grabherr, R., Schatzmayr, G., Haltrich, D., & Moll, W. D. (2010). Enhancement of solubility in Escherichia coli and purification of an aminotransferase from Sphingopyxis sp. MTA144 for deamination of hydrolyzed fumonisin B1. *Microbial Cell Factories*, *9*. https://doi.org/10.1186/1475-2859-9-62
61. Kumar, M., Mommer, M. S., & Sourjik, V. (2010). Mobility of cytoplasmic, membrane, and DNA-binding proteins in Escherichia coli. *Biophysical Journal*, *98*(4), 552–559. https://doi.org/10.1016/j.bpj.2009.11.002
62. Mika, J. T., Schavemaker, P. E., Krasnikov, V., & Poolman, B. (2014). Impact of osmotic stress on protein diffusion in Lactococcus lactis. *Molecular Microbiology*. https://doi.org/10.1111/mmi.12800
63. Konopka, M. C., Sochacki, K. A., Bratton, B. P., Shkel, I. A., Record, M. T., & Weisshaar, J. C. (2009). Cytoplasmic protein mobility in osmotically stressed Escherichia coli. *Journal of Bacteriology*, *91*(1), 231–237. https://doi.org/10.1128/JB.00536-08

64. Sochacki, K. A., Shkel, I. A., Record, M. T., & Weisshaar, J. C. (2011). Protein diffusion in the periplasm of E. coli under osmotic stress. *Biophysical Journal*, *100*(1), 22–31. https://doi.org/10.1016/j.bpj.2010.11.044

Table 1: Diffusion Coefficients calculated from FRAP data for labeled BSA in PBS buffer at different bleach time durations

Bleach Pulse duration	k_1 ms^{-1}	k_2 ms^{-1}	a_1	a_2	p_1	p_2	τ_1	τ_2	$\tau_{1/2}$ (ave)	c_n µm	r_n µm	c_e µm	r_e µm	$D_{confocal}$ $\mu m^2 s^{-1}$
10ms	0.16	0.012	736	241	0.75	0.25	0.004	0.058	0.0056	0.54	0.74	1.15	1.59	68.5
10ms	0.16	0.013	1125	307	0.78	0.21	0.004	0.053	0.0054	0.54	0.74	1.15	1.59	71.2
63ms	0.046	0.005	726	359	0.67	0.33	0.015	0.14	0.0214	0.92	1.27	2.05	2.83	54.9
63ms	0.044	0.005	770	373	0.67	0.33	0.016	0.14	0.0222	0.92	1.27	2.05	2.83	54.2
63ms	0.046	0.005	466	254	0.65	0.35	0.015	0.13	0.0219	0.92	1.27	2.05	2.83	56.3

The rate constants (*k*) and amplitudes (a) are from the double-exponential fit of the FRAP data. The *c* values were obtained from Gaussian fits using equation 5. The respective radius (r) are calculated assuming the respective bleach circles diameter lies at 60% height from the bottom of the Gaussian Profiles (r=1.38**c*).

Table2: Key resources

Reagent Type(Species) or resource	Designation	Source or reference	Identifiers	Additional Information
PBS buffer	Dulbecco's phosphate buffered saline (PBS 1X)	Biological Industries	Catalog no. 02-023-1A	Sterile , Tissue Culture Grade
HEPES buffer	HEPES	Fisher BioReagents	LOT 170358	Molecular Biology Grade
Labelling Dye	CF514	Biotium	CF®514 Dye Alternative green fluorescent dye	
DMEM (MEDIA)	DMEM(1X) Gibco	Biological Industries	REF#41965-039	
Fetal Bovine Serum	FBS (Gibco)	Invitrogen	REF#12657-029	
Trypsin-EDTA	Trypsin-EDTA Solution A	Biological Industries	REF#03-050-1B	
Penicillin/ Streptomycin	Pen-Strep Solution	Biological Industries	REF#03-031-1B	
Pyruvate	Sodium Pyruvate Solution	Biological Industries	REF#03-042-1B	
Glass Dishes (For cell culture)	35-mm glass-bottomed dishes	MatTek Corporation	P35G-0-14-C	Uncoated
Dye Removal Columns	Pierce™ Dye Removal Columns	Thermo-Fisher scientific	Cat#22858	
Dialysis Tube	Gebaflex tubes 3.5KDa (GeBa)	TIVAN BIOTECH	Cat#MIDI3-100	
Glass Capillaries	Capillary Glass Tubing	Warner Instruments	Model No. G120TF-4 203-776-0664	Borosilicate-Thin wall with Filament

614 **Figure Legends:**

615

616 **Figure 1:** (A) Line-FRAP performed in a CFP transfected HeLa cell. White line represents the
617 scanning line; Red circular area denotes the bleaching area. (B): A single scanning line as a
618 function of time (in vertical direction) including the bleach. The red rectangular marks the
619 region of interest (ROI), which was used for analysis. A zoomed view of Line-FRAP profile,
620 is also shown where horizontal rectangular area (red colored marks ROI) denotes the
621 fluorescence intensity as a function of length across the scanning line. (C): Average of 30 FRAP
622 recovery curves as a function of time. (N=30; Correlation coefficient R=0.98)
623
624

625 **Figure 2:** (A) Line FRAP profile of a precipitated (fixed) sample (BSA labeled with CF514
626 Dye in 30% Glycerol in PBS buffer) after 10 ms and 63 ms bleach pulse. Corresponding
627 recovery profiles over time are shown. (B): Nominal bleach areas (before and after the bleach)
628 for the precipitated samples. The green circular area marked 2, denotes the nominal bleach
629 done by the laser when 10, 20 and 63 ms bleach pulses were used and the red circular area 1
630 denotes the bleach area defined by the clip tornado of 4 pixel (Inherent laser settings defined
631 by Olympus confocal system). (C-E): Determination of nominal bleach radius (rn) from the
632 fluorescence intensity profiles for (C) 10, (D) 20 and (E) 63 ms bleach pulse fitted using a
633 Gaussian equation. (N=20; R=0.99 for each of the fits)
634
635

636 **Figure 3:** (A) Fluorescence recovery (FRAP) after photobleaching of BSA labelled with
637 CF514 in PBS. Comparative data of 10 and 63 ms bleach pulse fitted to double exponential
638 equation are shown. (N=30; R=0.91 for 10ms and 0.97 for 63ms fit) (B-D): Determination of
639 effective bleach sizes from the fluorescence intensity profiles for 10 and 63 ms bleach pulse.
640 (B) single run data, (C) average of 30 measurements. (D) Gaussian fits for the average bleach
641 sizes after 10 and 63 ms bleach pulse. (N=30; R= 0.99 for both of the fits)
642
643

644 **Figure 4:** (A,C) FRAP recovery profiles for 10 and 63 ms bleach pulses of labeled BSA in PBS
645 buffer in the presence of 5, 10, 15 and 20% PEG8000. (N=30 for all; R= 0.96 for 5, 0.97 for
646 10, 0.98 for 15 and 20% fits in A) (R= 0.98 for 5%, 0.99 for rest of the fits in C) (B, D) Average
647 post bleach size of fluorescence intensity profiles after 10 ms (N=30 for all; R= 0.99 for each
648 of the fits in B) and 63 ms bleach pulses fitted to a Gaussian equation. (N=30 for all; R= 0.98
649 for 5% and 0.99 for rest of the fits in D) (E): Diffusion Coefficients (in µm2s-1) as a function
650 of Relative viscosity (η0 of water considered as 1, data are from panels A-D, final error bars
651 are calculated after combining all the individual errors from the respective average fits).
652
653

654 **Figure 5:** (A-C) FRAP recovery profiles of (A) E-fts (N=25; R=0.98) (B) baeR proteins (N=30;
655 R=0.98) labeled with CF514 dye in PBS buffer. (C) Corresponding averaged post bleach size
656 profiles for E-fts and baeR proteins fitted to a Gaussian equation (N=100; R=0.99). (D-G):
657 FRAP recovery profiles of (D) E-fts fused with YFP (N=30; R=0.99) (F) baeR fused with YFP
658 (N=30; R=0.99) in PBS buffer solution. Gaussian fits of averaged post bleach size profiles for
659 (E) E-fts fused with YFP (N=30; R=0.99) (G) baeR fused with YFP (N=30; R=0.99).
660

Figure 6: (A) A typical HeLa cell after successful micro-injection with a fluorescent labeled E-fts protein. (B-C): FRAP recovery profiles of (B) E-fts fused with YFP (N=43; R=0.99) (C) baeR fused with YFP (N=42; R=0.99) in HeLa cell cytoplasm. (D-E): Gaussian fits of averaged post-bleach size profiles for (D) E-fts fused with YFP (N=29; R=0.99) (E) baeR fused with YFP (N=36; R=0.99) in HeLa cell cytoplasm.

Figure 7: (A) Typical E.Coli cells after expression of YFP fused E-fts protein. (B, C): FRAP recovery profiles of (B) E-fts fused with YFP (N=49; R=0.99) (C) baeR fused with YFP (N=52; R=0.99) in E.coli cytoplasm. (D, E): Gaussian fits of post bleach size profiles for (D) E-fts fused with YFP (R= 0.98) (E) baeR fused with YFP (R= 0.97) in E.coli cytoplasm.

Figure 8: Comparing diffusion coefficients of E-fts and baeR proteins chemically labeled or fused with YFP in PBS buffer, HeLa cell cytoplasm and E.coli bacteria cells. (Final error bars are calculated after combining all the individual errors from the respective average fits).

Figure 9: (A) Normalized FRAP recovery profiles (N=20; R=0.97 for YFP in 2YT, N=30; R=0.98 in 150mM, N=30; R=0.99 in 300mM and N=30; R=0.99 in 500mM NaCl). (B) Corresponding Gaussian fits of averaged post-bleach size profiles (R=0.98 for YFP in 2YT, R=0.99 for 150mM, 300mM and 500mM NaCl). And (C) Comparison of diffusion coefficients for YFP protein expressed in E.coli cells under different osmotic stress environments (final error bars are calculated after combining all the individual errors from the respective average fits).

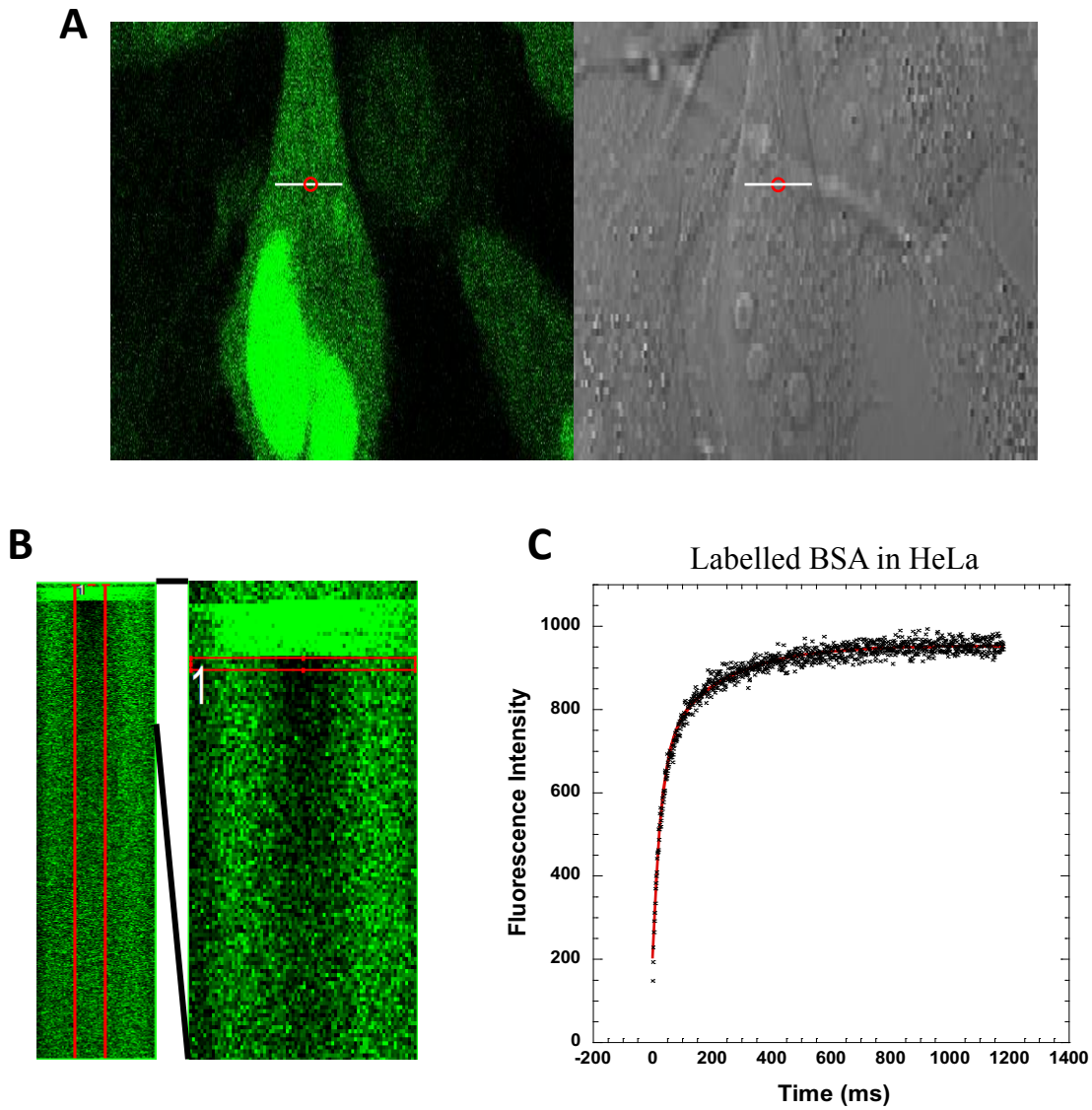

Figure 1: (A) Line-FRAP performed in a CFP transfected HeLa cell. White line represents the scanning line, Red circular area denotes the bleaching area. (B): A single scanning line as a function of time (in vertical direction) including the bleach. The red rectangular marks the region of interest (ROI), which was used for analysis. A zoomed view of Line-FRAP profile, is also shown where horizontal rectangular area (red colored marks ROI) denotes the fluorescence intensity as a function of length across the scanning line. (C): Average of 30 FRAP recovery curves as a function of time. (N=30;Correlation coefficient R=0.98)

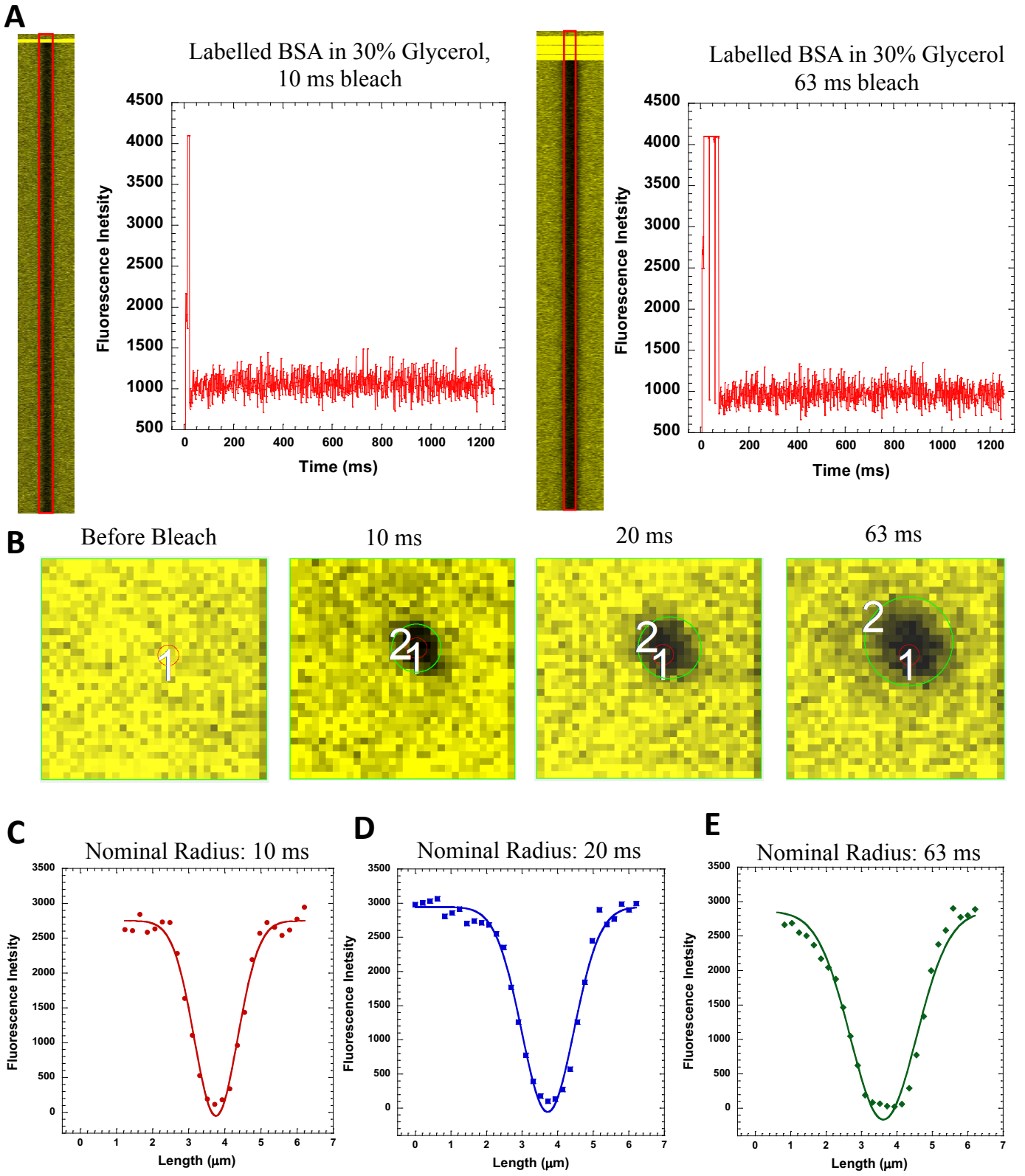

Figure 2: (A) Line FRAP profile of a precipitated (fixed) sample (BSA labeled with CF514 Dye in 30% Glycerol in PBS buffer) after 10 ms and 63 ms bleach pulse. Corresponding recovery profiles over time are shown. (B): Nominal bleach areas (before and after the bleach) for the precipitated samples. The green circular area marked 2, denotes the nominal bleach done by the laser when 10, 20 and 63 ms bleach pulses were used and the red circular area 1 denotes the bleach area defined by the clip tornado of 4 pixel (Inherent laser settings defined by Olympus confocal system). (C-E): Determination of nominal bleach radius (r_n) from the fluorescence intensity profiles for (C) 10, (D) 20 and (E) 63 ms bleach pulse fitted using a Gaussian equation. (N=20; R=0.99 for each of the fits)

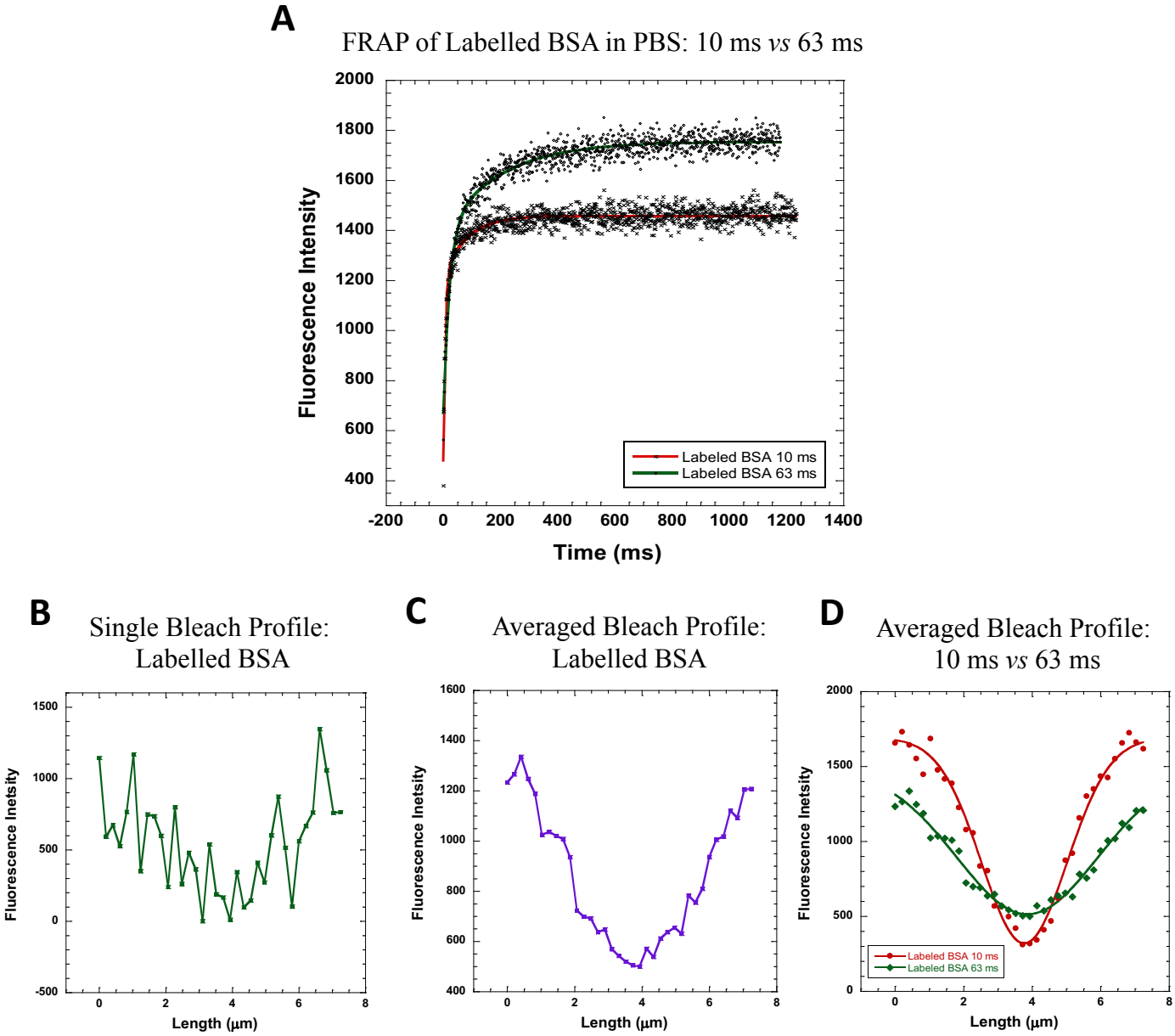

Figure 3: (A) Fluorescence recovery (FRAP) after photobleaching of BSA labelled with CF514 in PBS. Comparative data of 10 and 63 ms bleach pulse fitted to double exponential equation are shown. (N=30; R=0.91 for 10ms and 0.97 for 63ms fit) (B-D): Determination of effective bleach sizes from the fluorescence intensity profiles for 10 and 63 ms bleach pulse. (B) single run data, (C) average of 30 measurements. (D) Gaussian fits for the average bleach sizes after 10 and 63 ms bleach pulse. (N=30; R= 0.99 for both of the fits)

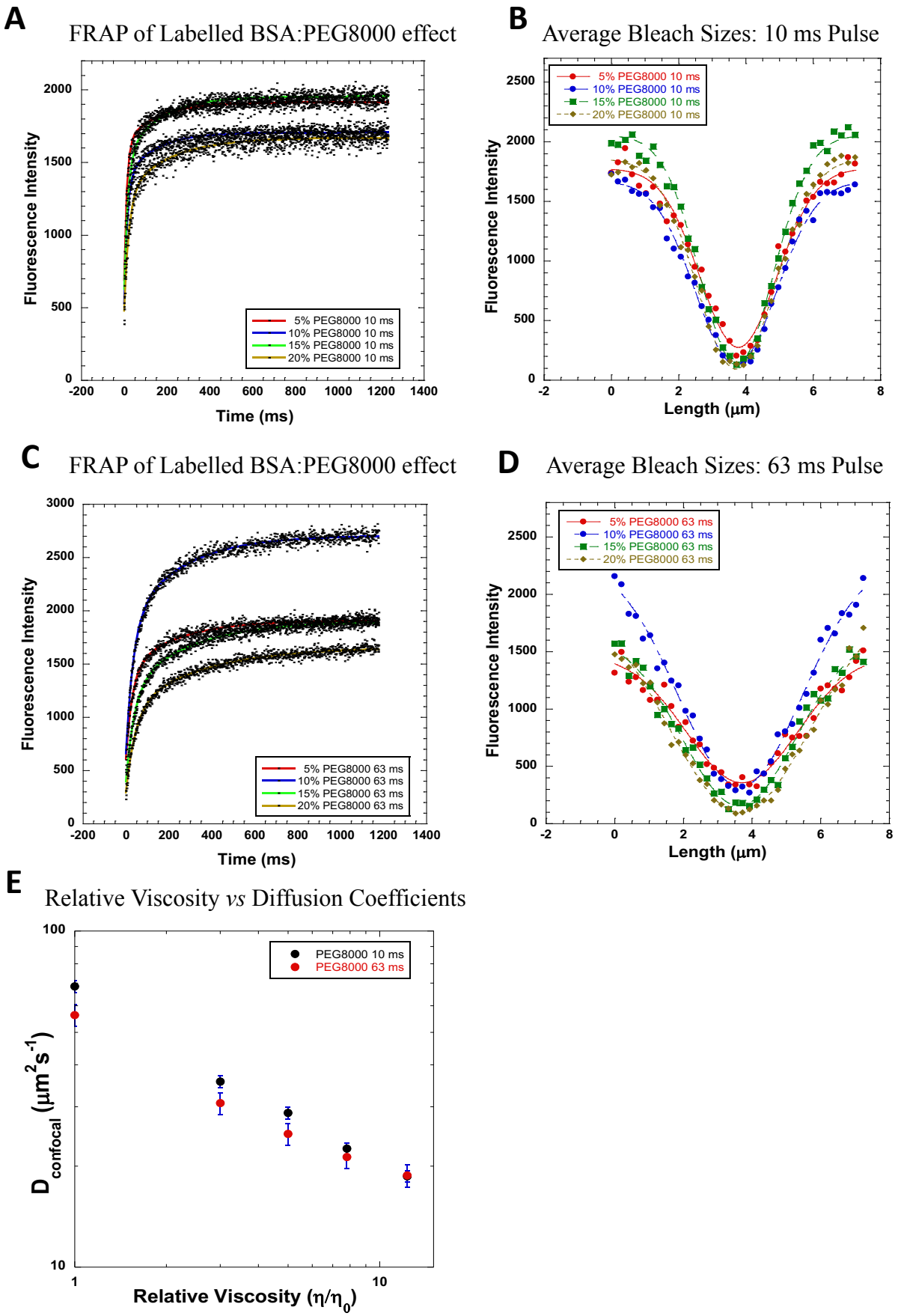

Figure 4: (A,C) FRAP recovery profiles for 10 and 63 ms bleach pulses of labeled BSA in PBS buffer in the presence of 5, 10, 15 and 20% PEG8000. (N=30 for all; R= 0.96 for 5, 0.97 for 10, 0.98 for 15 and 20% fits in A) whereas (R= 0.98 for 5%, 0.99 for rest of the fits in C) (B, D) Average post bleach size of fluorescence intensity profiles after 10 ms (N=30 for all; R= 0.99 for each of the fits in B) and 63 ms bleach pulses fitted to a Gaussian equation. (N=30 for all; R= 0.98 for 5% and 0.99 for rest of the fits in D) (E): Diffusion Coefficients (in $\mu m^2 s^{-1}$) as a function of Relative viscosity (η_0 of water considered as 1, data are from panels A-D, Final error bars are calculated after combining all the individual errors from the respective average fits).

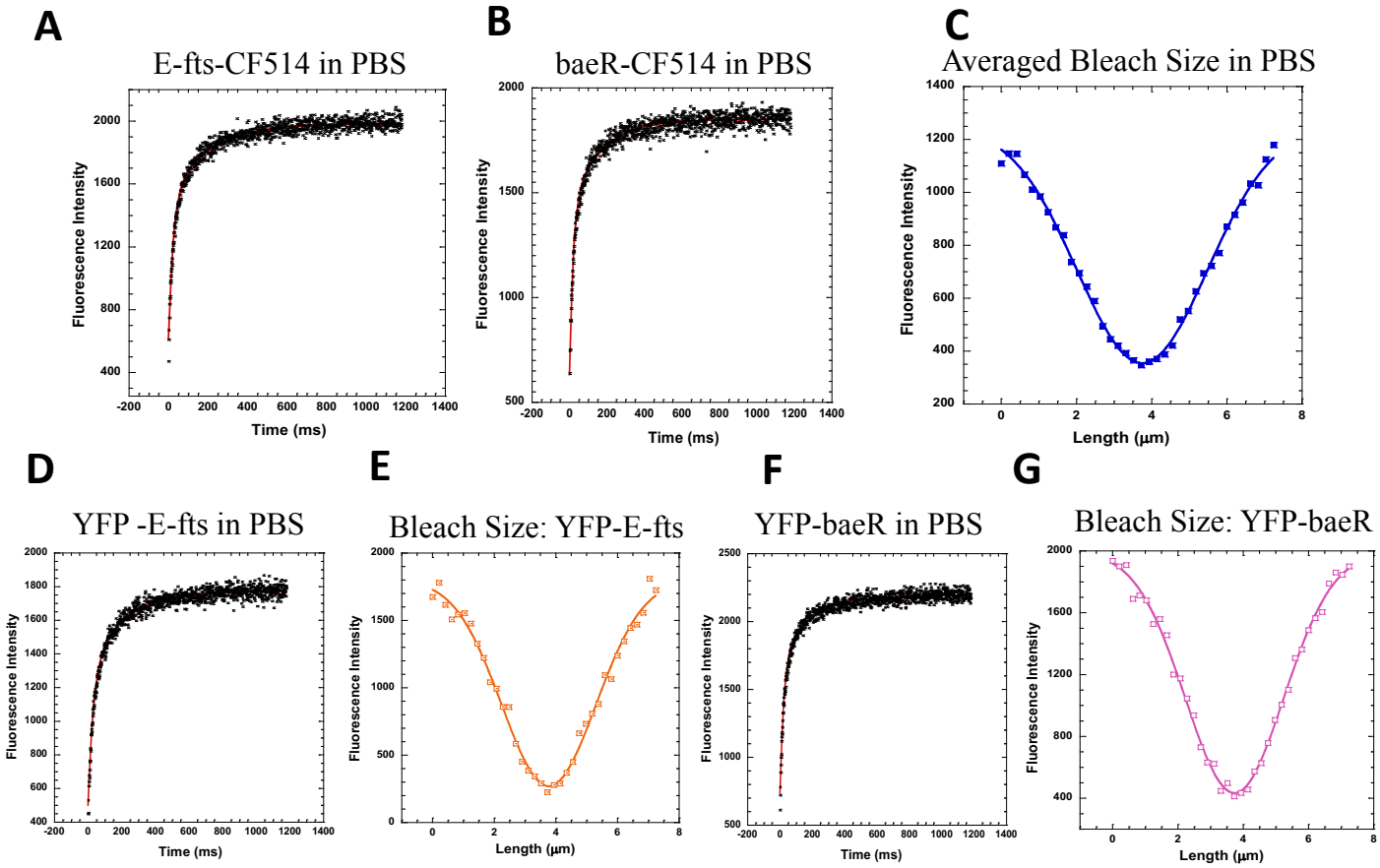

Figure 5

Figure 5: (A-C) FRAP recovery profiles of (A) E-fts (N=25; R=0.98) (B) baeR proteins (N=30; R=0.98) labeled with CF514 dye in PBS buffer. (C) Corresponding averaged post bleach size profiles for E-fts and baeR proteins fitted to a Gaussian equation (N=100; R=0.99). (D-G): FRAP recovery profiles of (D) E-fts fused with YFP (N=30; R=0.99) (F) baeR fused with YFP (N=30; R=0.99) in PBS buffer solution. Gaussian fits of averaged post bleach size profiles for (E) E-fts fused with YFP (N=30; R=0.99) (G) baeR fused with YFP (N=30; R=0.99) .

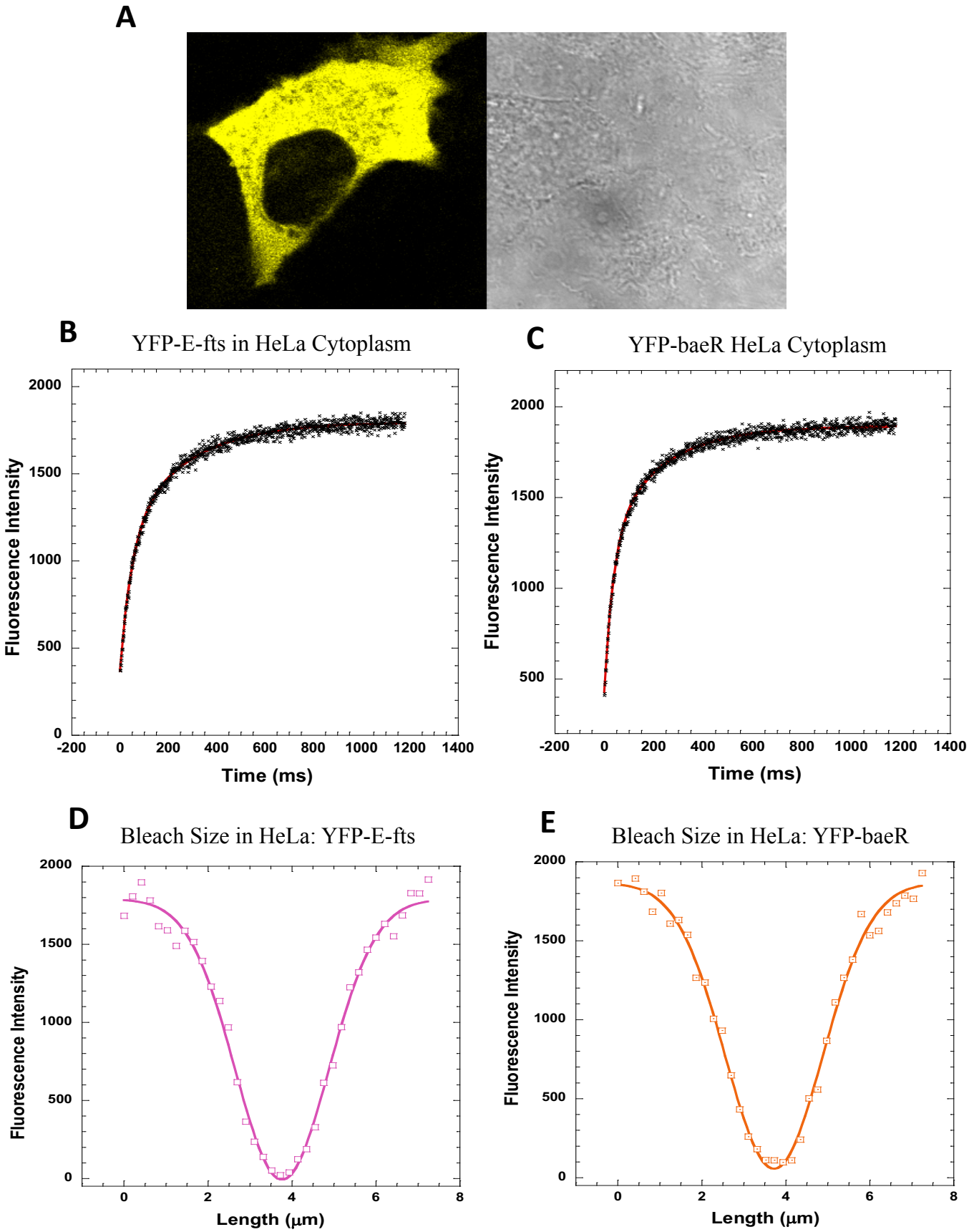

Figure 6: (A) A typical HeLa cell after successful micro-injection with a fluorescent labeled E-fts protein. (B-C): FRAP recovery profiles of (B) E-fts fused with YFP (N=43; R=0.99) (C) baeR fused with YFP (N=42; R=0.99) in HeLa cell cytoplasm. (D-E): Gaussian fits of averaged post-bleach size profiles for (D) E-fts fused with YFP (N=29; R=0.99) (E) baeR fused with YFP (N=36; R=0.99) in HeLa cell cytoplasm.

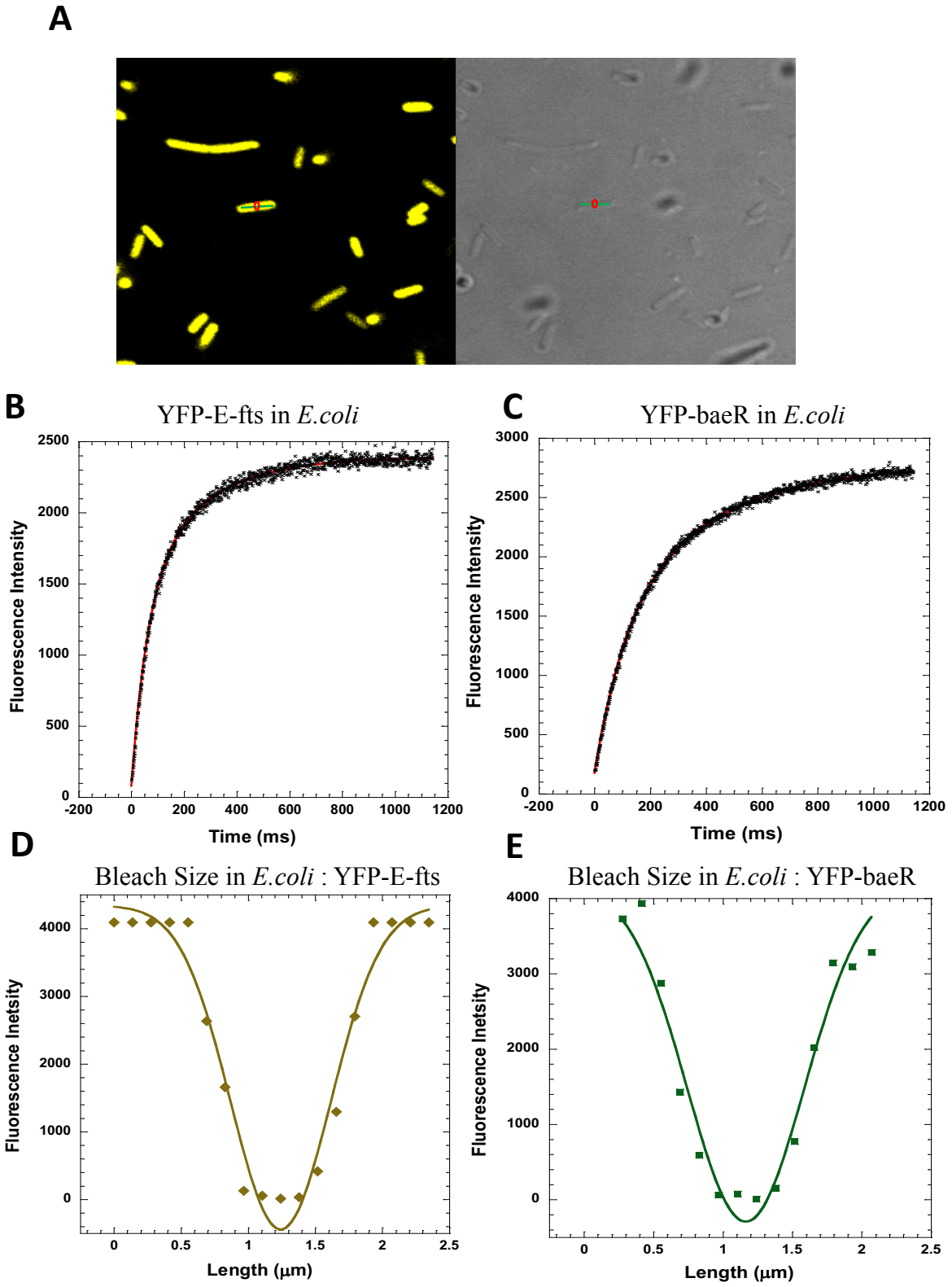

Figure 7: (A) Typical *E.Coli* cells after expression of YFP fused E-fts protein. (B, C): FRAP recovery profiles of (B) E-fts fused with YFP (N=49; R=0.99) (C) baeR fused with YFP (N=52; R=0.99) in *E.coli* cytoplasm. (D, E): Gaussian fits of post bleach size profiles for (D) E-fts fused with YFP (R= 0.98) (E) baeR fused with YFP (R= 0.97) in *E.coli* cytoplasm.

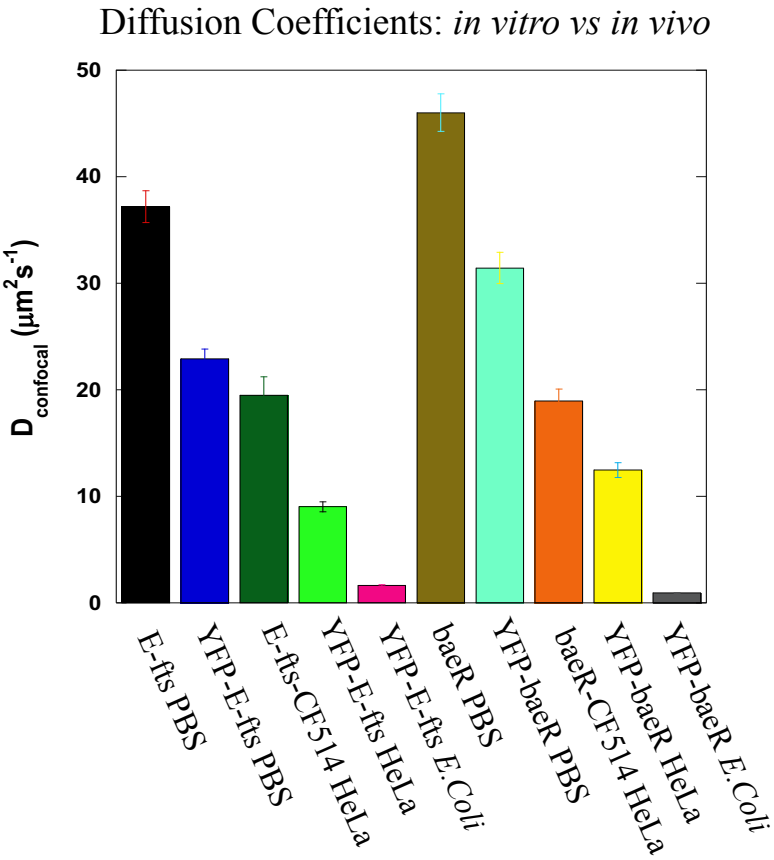

Figure 8: Comparing diffusion coefficients of E-fts and baeR proteins chemically labeled or fused with YFP in PBS buffer, HeLa cell cytoplasm and *E.coli* bacteria cells. (Final error bars are calculated after combining all the individual errors from the respective average fits).

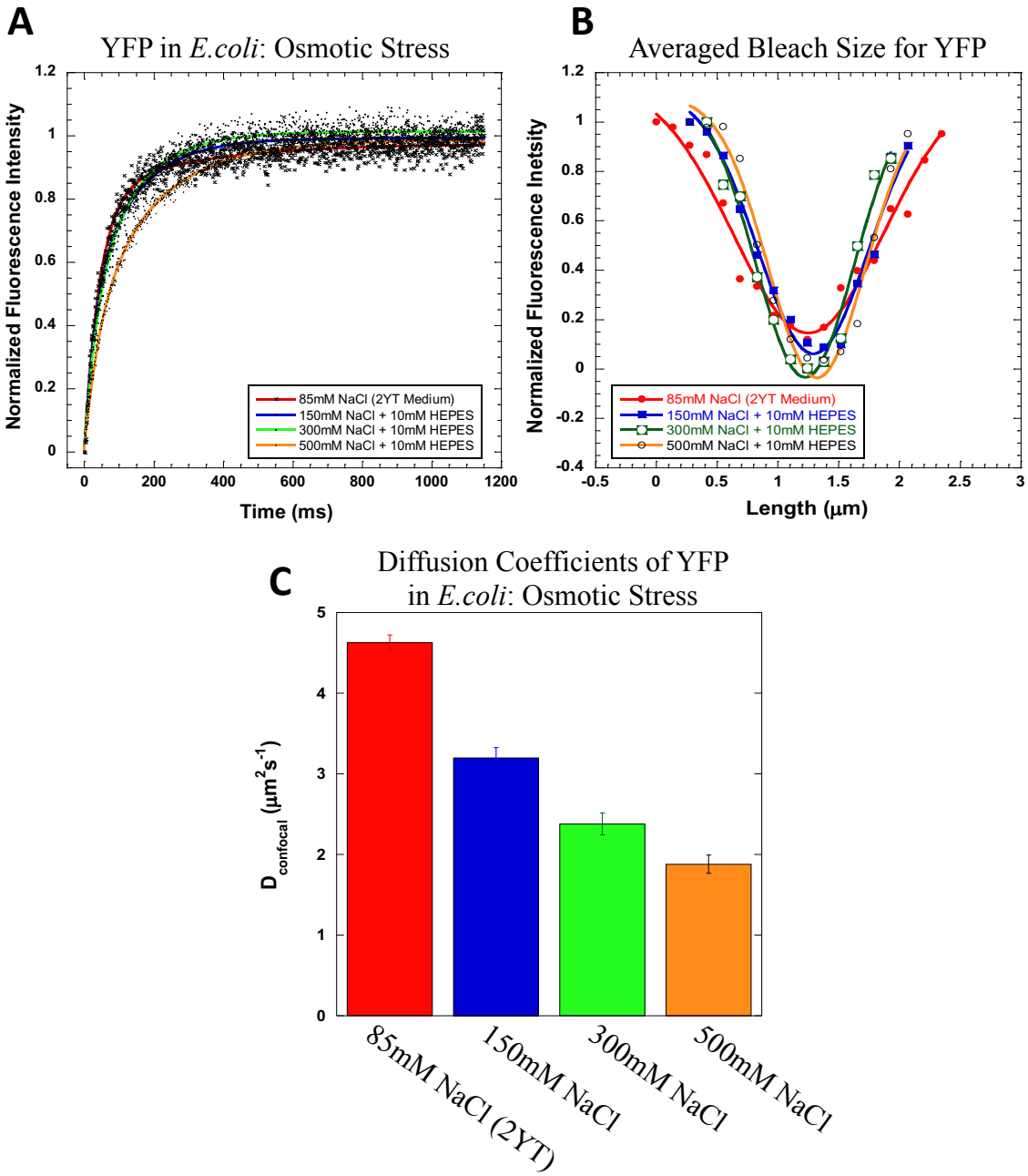

Figure 9: (A) Normalized FRAP recovery profiles (N=20;R=0.97 for YFP in 2YT, N=30;R=0.98 in 150mM, N=30;R=0.99 in 300mM and N=30;R=0.99 in 500mM NaCl) (B) corresponding Gaussian fits of averaged post-bleach size profiles (R=0.98 for YFP in 2YT, R=0.99 for 150mM, 300mM and 500mM NaCl) and (C) Comparison of diffusion coefficients for YFP protein expressed in *E.coli* cells under different osmotic stress environments (Final error bars are calculated after combining all the individual errors from the respective average fits).

.